Design and Fabrication of a Low-Cost Three-Dimensional Bioprinter

Colton McElheny
Department of Mechanical Engineering,
Louisiana State University,
Baton Rouge, LA 70803

Daniel Hayes
Department of Biomedical Engineering,
Pennsylvania State University,
University Park,
State College, PA 16802

Ram Devireddy[1]
Department of Mechanical Engineering,
Louisiana State University,
2508 P.F. Taylor Hall,
Baton Rouge, LA 70803
e-mail: devireddy@me.lsu.edu

Three-dimensional (3D) bioprinting offers innovative research vectors for tissue engineering. However, commercially available bioprinting platforms can be cost prohibitive to small research facilities, especially in an academic setting. The goal is to design and fabricate a low-cost printing platform able to deliver cell-laden fluids with spatial accuracy along the X, Y, and Z axes of 0.1 mm. The bioprinter consists of three subassemblies: a base unit, a gantry, and a shuttle component. The platform utilizes four stepper motors to position along three axes and a fifth stepper motor actuating a pump. The shuttle and gantry are each driven along their respective horizontal axes via separate single stepper motor, while two coupled stepper motors are used to control location along the vertical axis. The current shuttle configuration allows for a 5 mL syringe to be extruded within a work envelope of 180 mm × 160 mm × 120 mm (X, Y, Z). The shuttle can easily be reconfigured to accommodate larger volume syringes. An attachment for a laser pen is located such that printing material may be light-activated pre-extrusion. Positional fidelity was established with calipers possessing a resolution to the nearest hundredth millimeter. The motors associated with the X and Y axes were calibrated to approximately 0.02 mm per motor impulse. The Z axis has a theoretical step distance of ~51 nm, generating 0.04% error over a 10 mm travel distance. The A axis, or pump motor, has an impulse distance of 0.001 mm. The volume extruded by a single impulse is dictated by the diameter of the syringe used. With a 5 mL syringe possessing an inner diameter of 12.35 mm, the pump pushes as little as 0.119 μL. While the Z axis is tuned to the highest resolution settings for the motor driver, the X, Y, and A axes can obtain higher or lower resolution via physical switches on the motor drivers. [DOI: 10.1115/1.4037259]

Keywords: bioprinting, biomedicine, 3D printing, microextrusion, tissue engineering, cells

Introduction

Tissue and organ failure due to trauma, disease, or aging accounts for hundreds of billions of dollars in national healthcare costs in the U.S. alone. In 2012, there were 118,520 patients on the organ recipient waiting list with only 28,432 transplant operations performed. Additionally, 8,420 patients died waiting for organs, while another 3,250 patients were too sick to undergo an operation when an organ became available [1]. Tissue engineering may help with this unmet need by offering alternative or complimentary avenues to address organ/tissue failure via development of natural, synthetic, and natural–synthetic hybrid biomimetic tissue and organ surrogates [2]. Traditionally, cellular scaffolds are prefabricated and then seeded with cells forming tissue-engineering constructs. On the cellular level, the cell is still experiencing a two-dimensional (2D) culture, limiting its use as a biomimetic model [3]. Beyond the limitations of recreating a true three-dimensional (3D) microenvironment, vascularizing large constructs remains problematic. Oxygen diffusion becomes ineffectual for constructs with cells more than 200 mm from a source, either vascular or media/construct–atmosphere interface [4,5]. With such intrinsic challenges connected to traditional scaffold development and cellular association, tissue engineering is undergoing a paradigm shift, adopting methodologies more associated with the electronics industry than biotechnology.

In the last 12 years, additive manufacturing (AM) has become a new frontier for tissue engineers to explore. AM in bioengineering presents not only a paradigm breaking approach for the construction of tissue constructs but also a clear and feasible path toward up-scalable, high throughput, and personalized generation of medical implants. By adapting commercial AM processes to biomedicine, medical professionals can and have begun practicing truly individualized medicine [6]. The combination in personalized flexibility of design, as well as the reliability and reproducibility of automated assembly, engenders AM to the biomedical field [7].

Equally important in developing tridimensional cell interaction is proper material selection. Commercially available home 3D printers generally use plastics, such as acrylonitrile butadiene styrene or polylactide. Other rapid prototyping systems use resin, polymers, ceramics, powders, or metals to stack 2D layers into a 3D final product, utilizing organic solvents, high temperatures, or nonbiocompatible crosslinkers. Hydrogels present an ideal opportunity for bioprinting application to encapsulate cells within printed material [7–9]. Many hydrogels have been used in experimentation: collagen, gelatin, Matrigel, agarose, alginate, as well as many synthetic polymers [7]. Of these, alginate is one of the more common due to its favorable biocompatibility, cellular support capacity, and drug-delivery potential and has been successfully used with several cell types including mesenchymal stem cells, endothelial cells, neural cells, and hepatocytes [10–15].

Background and Prior Art

Several commercial units are available as well as platforms developed in-house with various research groups. However,

[1]Corresponding author.

Manuscript received May 26, 2016; final manuscript received June 24, 2017; published online August 7, 2017. Assoc. Editor: Xiaoming He.

low-cost devices with readily available components are lacking. A few systems which were considered as part of the design development process are mentioned.

BioScaffolder. The BioScaffolder developed by GeSim couples nonbiological pressure driven (100–800 kPa) microextrusion with optional piezoelectric cell deposition. It possesses 2 μm step sizes in the *X* and *Y* direction and 10 μm control in the *Z*. With an included heating pad, it can process biopolymers, hydrogels, bone cement paste, biocompatible silicones, and polymer pastes. It has a work envelope of 100 mm × 346 mm × 40 mm, allowing different configurations of culture dishes and plates.

Bioplotter. The Bioplotter by EnvisionTec operates at 0.1–150 mm/s that transverses a work envelope of 150 mm × 150 mm × 140 mm. The BioPlotter has a 0.001 mm resolution along the *X*, *Y*, and *Z* axis. Five unique material catridges can be used per job and the system maintains an automatic tool changer. It is also equipped with high and low temperature nozzles and switchable base plates to allow operational temperature ranging from 0 °C to 250 °C.

RepRap. RepRap is an open-source, low-cost home 3D printing platform. One of its main selling points is that once a main unit is set up, it is able to print and replace all of its mechanical parts. Work envelopes and resolution are system dependent as drive electronics can be upgraded to improve resolution. While the RepRap is a community-based open-source environment, it allows for a lot of flexibility in design. However, this comes at the price of each RepRap build being slightly different, increasing troubleshoot times. Additionally, the software controls for RepRap are developed with ARDUINO. While ARDUINO is a versatile I/O and language system, it does present another hurdle to overcome in the learning process.

Do-It-Yourself Computer Numeric Control Mills. Recognizing that 3D printers are similar to computer numeric control (CNC) devices with a print head instead of a drill tool, a great deal of insight could be gained from related forums. Additionally, CNC mills and lathes have long-standing industrial uses which have prompted the development of dedicated software for multiple axis control. Software such as MACH3, OMAX LAYOUT, or LINUXCNC made by third parties are designed to make utilizing CNC devices as user friendly as possible.

Inkjet Printers. Wilson and Boland [16] showed that stock inkjet printers could be modified for use as a bioprinter. Advances made in biomaterials have resulted in the enabling of 3D control [17]. Inkjet systems are the most cost effective, with the lowest end printers costing only $29.99 as of January 2015. With a commercial inkjet system, the power, X and Y motor control, and interfacing are already established. Additionally, 2D representations of a design can be loaded into basic home office software and printed without the need to purchase or learn new software. And while not necessarily being used for its originally intended purpose, Wilson and Boland [16] found that manufacturer technical support was willing to lend troubleshooting aid.

Absorbing Film-Assisted Laser-Induced Forward Transfer Bioprinting. Absorbing film-assisted laser-induced forward transfer bioprinting (AFA-LIFT) provided the most consistent, positive results of the laser-assisted bioprinting methods. Guillotin et al. [18] showed that high cell densities could be used to statistically print physiologically relevant cell concentrations with native tissue resolution. However, high upkeep, laborious sample preparations, and highly specialized equipment impose a substantial barrier to field entry.

Design Criteria

A cost-effective printing platform was designed to dispense a cell-laden cube measuring 1 cm × 1 cm × 1 cm with a minimal positional resolution goal of 100 μm and reasonable printing speed with future applications of the printing system intended to utilize mesenchymal stem cells, which in suspension exhibit a diameter of approximately 30 μm [19]. It is important to note that for a nozzle or orifice based approach, consideration must be taken of the need to allow cells to pass through without clogging or exposure to undue shear stress. Furthermore, as with all bioprinting platforms, cell viability should be as high as possible, with a lower end goal of 70% viability; any viability value lower than 70% could have potential negative consequences for cell differentiations and associated necrotic/apoptotic response. The bioprinter was developed as a cost-effective tool for a small-scale academic research lab. It is stored and operated in a biological safety cabinet. The cabinet has workable envelope of 70 in. × 20 in. × 27 in. ($W \times D \times H$) necessitating a smaller footprint for the device. The platform is portable and constructed of clear acrylic that is sterilized via ethylene oxide gas saturation. This is of particular relevance since academic research laboratory groups experience higher turnover and greater temporary employment than most dedicated research facilities. With the influx of untrained assistants, being able to visually inspect a mainly stationary system for signs of contamination is advantageous.

Concept Generation, Evaluation, and Design Selection

Print Modality. The first decision to make with the development of the printing system was which modality to pursue. Initially, modifying an inkjet printer seemed to be the ideal choice. Low end thermal inkjet printers print a 600 dpi × 600 dpi resolution, allowing for ~1 μm resolution. However, this is managed via a print head nozzle of ~21 μm. Stem cells typically exhibit diameters of 20–30 μm across. While cells are able to undergo significant deformation, the shear stresses of ejecting cells through an opening two-thirds their size could prove catastrophic. While there is the potential that the cells will be able to recover from this stress, no literature was found to support this. As viability is one of stipulated design goals, this uncertainty removes inkjet technology from design considerations.

With cell viability excluding inkjet technologies from consideration, the next best choice seemed to be AFA-LIFT. Guillotin and Guillemot [20] reported cell viability near 100% post print with single cell resolution at 5 kHz operating speed. Furthermore, the use of a laser system for cell deposition could be utilized as a catalyst for the light-initiated differentiation of human adipose tissue derived adult stem cells into bone [21]. However, laser-assisted bioprinting systems are expensive and are over-engineered for the intended immediate use of this system. The disadvantages of a laser-assisted bioprinting setup also include maintenance, laborious sample preparations, and steep learning curves.

Microextrusion is a relatively inexpensive option for 3D printing. Dependent on extrusion methods, cell viability ranges of 40–95% have been achieved [22–24]. Nonbiological 3D microextrusion printing have even recorded a resolution of 5 μm and linear speed of at 50 μm s^{-1}, comparable to laser-assisted systems [22]. Microextrusion has also successfully incorporated the standard materials of 3D printing, such as acrylonitrile butadiene styrene plastic or polylactide plastic, as well as several biologically relevant materials such as hydrogels, biocompatible copolymers, and cell aggregates with viscosities ranging from 30 to 6 × 10^8 mPa/s [25,26]. Depending on the system configuration, microextrusion printing has a resolution ranging from five micrometers to millimeters wide deposition. Second only to inkjet technologies, microextrusion has fairly simple sample preparation protocols, decent throughput potential, and is easy to learn. With sufficient resolution, manageable costs, and excellent viability

potential, microextrusion was the chosen modality to design the printing platform.

Material Selection. Poly(methyl methacrylate), also known as acrylic or PMMA, is a strong, light-weight thermoplastic that can be easily machined. Acrylic sheets also resist ultraviolet light degradation seen with other clear plastics. While optically clear, acrylic does block wavelengths below 400–300 nm. While the working area will be sterilized, UV sterilization is prevented on interior surfaces. However, this is the same issue stainless steel or aluminum would face. With acrylic though, if a bacterial or fungal colony develops outside the UV sterilization range, it will be visually apparent to the end-user.

The gold standard for biological sterilization is autoclaving in which specimens are subjected to saturated steam under a pressure of approximately 15 PSI reaching temperatures of at least 121 °C. Many plastics, PMMA included, exhibit glass transition temperatures, which are temperature ranges in which a polymer transitions from a hard, rigid material to a soft, elastic material. Acrylic undergoes this switch over the range of 85–165 °C based on the copolymer composition. As such, dependent on the manufacturer, PMMA could be subjected to autoclaving. However, other sterilization methods, such as ethylene oxide gas saturation, may provide an alternative with lower temperature and pressure profiles allowing for more stable and repeatable results.

Axial Actuation. Acrylic is a fairly light-weight material with a density of 0.0434 lb/in^3. Assuming stepper motor use, many NEMA-23 stepper motors weigh between 1.5 and 2.5 lb. With a four- or five-axis system, motor weight would still only account for a maximum of 12.5 lb. Doubling this value for total weight of the heaviest part should allow for a conservative estimate to determine if stepper motors or servomotors are most appropriate. With an idealized inch per minute of 500 in/min, the watts required are 23.54 W. If the required watts are below 100 W, then the load setup is well within the range of stepper motor function. Above 200 W would require the power output of servo motors, while in between the two values would be at the top end of stepper motor functionality and the low end of servomotor domain. Our calculations show that for this bioprinter application, lower-end stepper motors are appropriate, and that servomotors would be completely unsuitable.

Control Program. Along with stepper motors, a breakout board, power supply, and stepper motor drivers are necessary for design inclusion. Many breakout boards facilitate direct communication between the CNC software running on a computer and the stepper motor drivers. This can cause issues with many modern computer systems as DB-25 parallel port connections are becoming rarer. Unfortunately, using a USB to DB-25 parallel port adapter is not a viable solution. Parallel ports facilitate direct communication between the computer and the stepper motor drivers. Both the signal frequency and the signal amplitude convey input parameters for stepper motor coordination. While USB to DB-25 converts the signal, proper signal timing is lost.

The pulses are generated based on the computer's internal central processing unit clock, which in turn is based on its kernel processing speed. This means that when the central processing unit slows down due to heavy processing cycles, the timing of the pulses will lag behind as well. To reduce the chance of this occurrence, desktop computers should be used over laptops due to their more stable power supply and a dedicated system should be used for processing and actualizing jobs. Another concern with stepper motor use is basic interfacing errors due to driver firmware/computer software incompatibility. Driver firmware should be flash updated and synced with the CNC controller. With this in mind, a four-axis stepper motor kit was selected for use with MACH3 firmware already installed.

MACH3 is a CNC software usually dedicated to mills, lathes, or plasma cutters. However, MACH3 has a very active community, many of which are interested in expanding their mill utility into potential 3D printing. One such community member, Nuri Erginer, developed an add-on to the MACH3 program that translates a fourth axis, the A axis, as an extruder. Calibration is required to translate the linear distance of an extruded filament into the volumetric extrusion from a pump; however, it is a quick and viable solution to avoid a potential laborious coding concern. The add-on to MACH3 decomposes STL model files in printable layers and then generates and posts G-CODE to MACH3. G-CODE is the programing language utilized by stepper motors to map and execute pathing. The combination of MACH3 and modified code mitigates the need to learn a new programing language to successfully operate the bioprinter.

Printer Configuration. With the structural material and drive components determined, the overall configuration of the platform needs to take shape. For this novel system, two structures on either side of the working envelope support a carriage that is able to traverse the *Y*-plane (see Fig. 1). These two structures are able to travel along to *X*-plane, imparting 2D control. These side pieces also allow the gantry to travel in both directions along the *Z* axis imparting full tridimensional positioning capability. Within the gantry, a syringe pump extrudes cell-laden fluids into a waiting substrate. The base is held stationary to mitigate tidal and inertial forces experienced by the substrate associated with moving the substrate.

The bioprinter has a working area large enough to manage common culture containers such as Petri dishes, multiwell culture plates, centrifuge tubes or glass slides, and cover slips. To establish reasonable print speeds, open-ended miniature extra light (MXL), 1/4 in wide timing belts are used to drive the gantry in the *X* and *Y* directions. Loops were created on the terminal ends of the timing belts via drilling a #4 machine screw through the center of the belt and clamping it tight between two #4 washers and secured with a nut. The Kevlar reinforcing fibers were able to maintain belt tensile strength, allowing the stepper motor to pull the gantry back and forth along the two axes. To generate movement along the *X*-axis, the MXL timing belt is linked around a cap screw in the gantry support, threaded around a timing-pulley coupled to the drive shaft, passed through the center of the gantry support structure, circled around an idler pulley on the opposite end of the work area, and held in place by another cap screw in the gantry. The *Y*-axis belt passes through an opening in the shuttle, redirected by two ten-tooth idler pulleys, connected to a 20-tooth MXL pulley directly coupled to a stepper motor, diverted by another two idler pulleys to loop around a vertical cap screw on the opposite side of the gantry.

While printing may transverse several inches along the *X* and *Y* axis in a single command, the *Z* direction will only raise a fraction of that height before another layer is deposited in the *XY* plane. Dependent on pump flow rates, the diameter of the extruded fluid, and thus the Z intervals, may be on the order of a few micrometers. This necessitates a higher resolution, reproducible method of controlling the *Z* axis position. A leadscrew application allows for greater control than belt actuated movement. A coupling nut, restricted from rotational movement, is easily implemented for such a task. With a 1/4 in 20 thread coupling nut and a stepper motor with a 200 step/revolution resolution, a 6.35 μm step travel distance is achieved. The stepper motor drivers also offer the option for microstepping, a method for increasing motor resolution at the cost of travel speed. Microstepping increases the requisite pulses per revolution via jumper resistor manipulation. The proper configuration allows these stepper motor drivers to change from 200 steps per revolution to 25,000 steps per revolution.

Four motors were used to actuate 3D control. Two of the motors power vertical movement due to the torque associated

Fig. 1 Representative photographs of the final assembled device within the Bio-Safety Cabinet

with two drive shafts on distal ends of such a wide work area, while the *X* axis and *Y* axis are each controlled by a single motor. The design has a gantry of approximately 22 lb that imposes variable torque on the stepper motors due to the print head's relative position along the *Y*-axis. While a belt was initially considered to couple the two drive shafts, issues with maintaining belt tightness and step cohesion prompted a change in design. There are multiple ways to couple the two *Z* axis motors both physically and via software. Due to the constraints of working with a four-axis break out board, physical coupling via wiring was chosen. By wiring the two motors, and each of the solenoid driving coils, to be in parallel with each other, the load tolerance of the motors was essentially doubled. The parallel wiring mitigates the current values that power each coil, reducing power generation at lower speeds. While not ideal, this does not overtly impact the printing procedure due to the limited travel distance between layer depositions.

A fifth motor acts as a pump to extrude material into a substrate of interest. This motor is a noncaptive stepper motor that allows a M10-2 threaded rod to pass all the way through it with a native 10 μm step distance. A flanged shaft collar and linear bearing constrain the threaded rod from rotation, inducing linear vertical movement. Extrusion occurs when the threaded rod extends downward from the motor, driving the plunger of a full syringe forward. With microstepping, the distance traveled by the plunger can be reduced to negligent. However, the inner diameter of syringe is a static variable and thus has the greatest impact on print resolution. Figure 1 shows several model views of the completed assembly, the base, gantry, and supporting structures.

Machining. A laser cutter was used to generate acrylic parts. Utilizing a 1 in working distance, the 60 W laser was inhibited to 0.1 speed and 30% power to cut through 0.475 in thick acrylic. For the thinner, 0.22 in pieces, the laser operated at 0.4 speed and 70% power. Most passes created clean cuts on the first attempt. Spatially large parts, such as the base parts, required multiple cuts. This is due to some minor flexing of the thinner acrylic that skewed the focal distance from the surface of the material, causing inefficient cuts. To overcome this, the laser cut the same path multiple times until a clean break occurred. Acrylic is a flammable thermoplastic and capable of combustion during laser cut procedures, in which a laser melts through the plastic to create separation. Passing the laser over previously exposed material increased probability of combustion and greater care needed to be exercised. Batch to batch variation was minimal allowing for use of uniform speed and power settings with only an occasional fine tuning of parameters to facilitate cleaner cuts.

Cross drilling was performed on a standard drill press equipped with micropositional encoders. A rotation-based edge-finder was

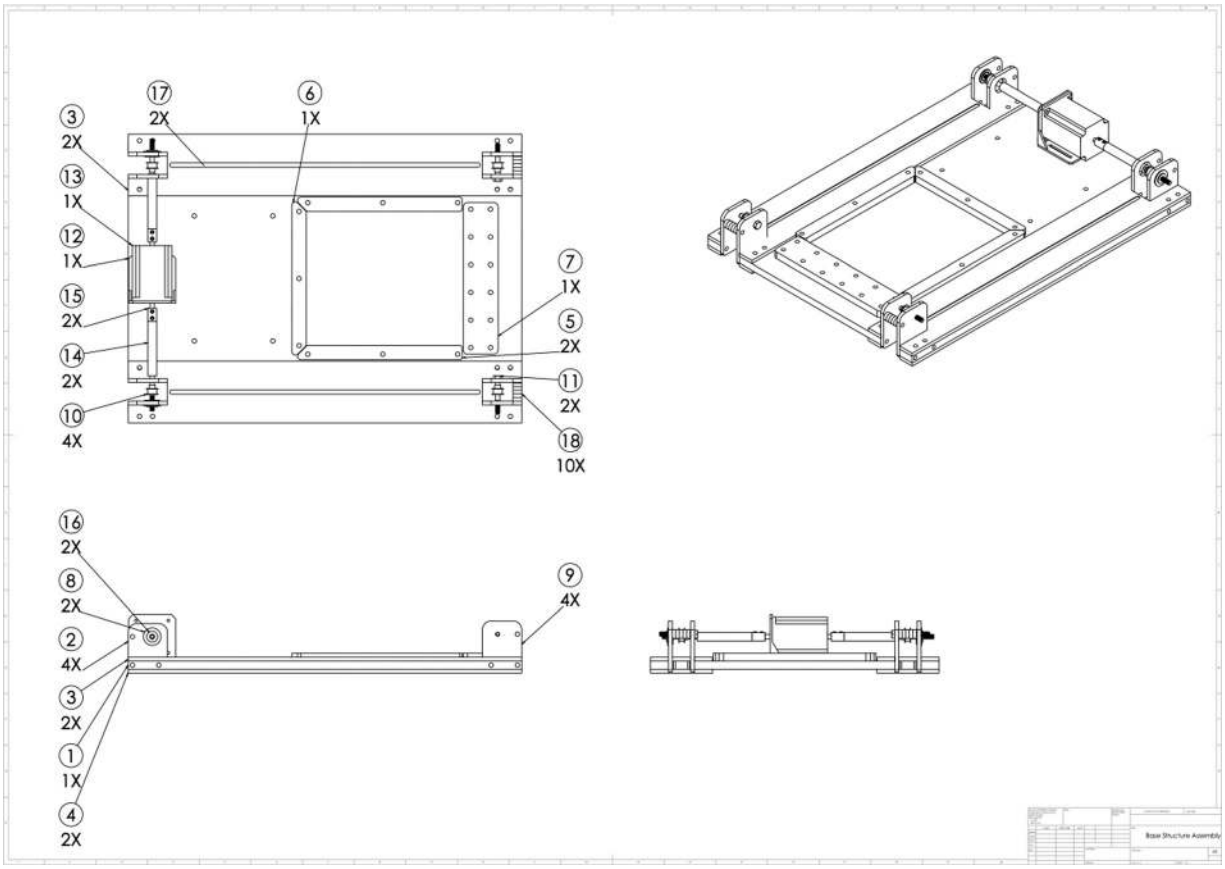

Fig. 2 Base assembly: The base assembly of the device, which includes a driving stepper motor with idler pulleys opposite it for *X*-axis control via timing belt, offers a work envelope of 7.5 in (190.5 mm) in the *X*-axis and 8.75 in (222.25 mm) in the *Y*-axis

used to identify the leading edge, then the encoder readout ensured accurate positioning in relation to the edge. Holes were also counter sunk using the same drill press. When available, a water-based coolant was used to manage thermal stresses from the drilling process. Otherwise, WD-40 was used as a coolant.

Assembly Features. The complete assembly utilizes just over 40 unique custom-designed parts occupying a footprint of 21.875 in × 15.09 in × 20.57 in (compared to the 70 in × 20 in × 27 in available space) and a working envelope of 7.1 in × 6.3 in × 4.75 in (180 mm × 160 mm × 120 mm). The motors can be tuned to accommodate a range of printing speeds and will need to be optimized for different printing criteria. In its fully assembled state, the entire platform weighs approximately 35 lb. The laser hangs below the carriage to activate cells within the syringe. This can easily be rearranged to shine vertically into the substrate in the case of heating or cooling pads obstructing the syringes optical clarity or other line of sight issues.

Maintenance. Many biological labs utilize various concentrations of ethyl alcohol for disinfection purposes. In the presence of this bioprinting platform, this practice needs to be modified. Alcohol induces stress crazing in PMMA, causing a network of cracks throughout its structure. As expected, the propagation of fracture networks in a structural material closely precedes defunct functionality. An alternative to alcohol sanitation is the use of dimethyl benzyl ammonium chloride. Twenty-four hour continuous exposure resulted in no visible change in a machined PMMA piece's appearance. Comparatively speaking, a machined piece exposed to 100% alcohol for the same time period showed significant surface crack presence. Other nonalcoholic based disinfecting products could be used as well.

Validation of Bioprinting Platform

Z-Axis Calculations. The *Z* axis motors are stressed the greatest due to working against gravity to drive the gantry vertically. Stepper motor is rated not by their power output, but by their holding torque. Additionally, rotor inertia should be ratio matched against the load inertia. Having too high of a ratio increases the risk of missed steps and severely limits motor functionality. As seen in Eq. (1), the total load inertia is the sum of the screw inertia and the structural load inertia. In Eq. (2), J_w is the inertia due to the weighted load, W is the weight in pound, and P_B is the screw pitch. For Eq. (3), ρ is the density of the steel used for the leadscrew, L_B is the length of the leadscrew, while D_B is the diameter of the screw

$$J_L = J_W + J_S \tag{1}$$

$$J_w = W * 16 * \left(\frac{P_B}{2\pi}\right)^2 \tag{2}$$

$$J_S = \left(\frac{\pi}{32}\right) * \rho * L_B * D_B^4 \tag{3}$$

Substituting these values into the above equations establishes: $J_W = 0.01116\ \text{oz}*\text{in}^2$, $J_S = 0.02102\ \text{oz}*\text{in}^2$, and $J_L = .03218\ \text{oz}*\text{in}^2$. For NEMA-23 motor sizes, the ratio defined in Eq. (4) should be no larger than 5

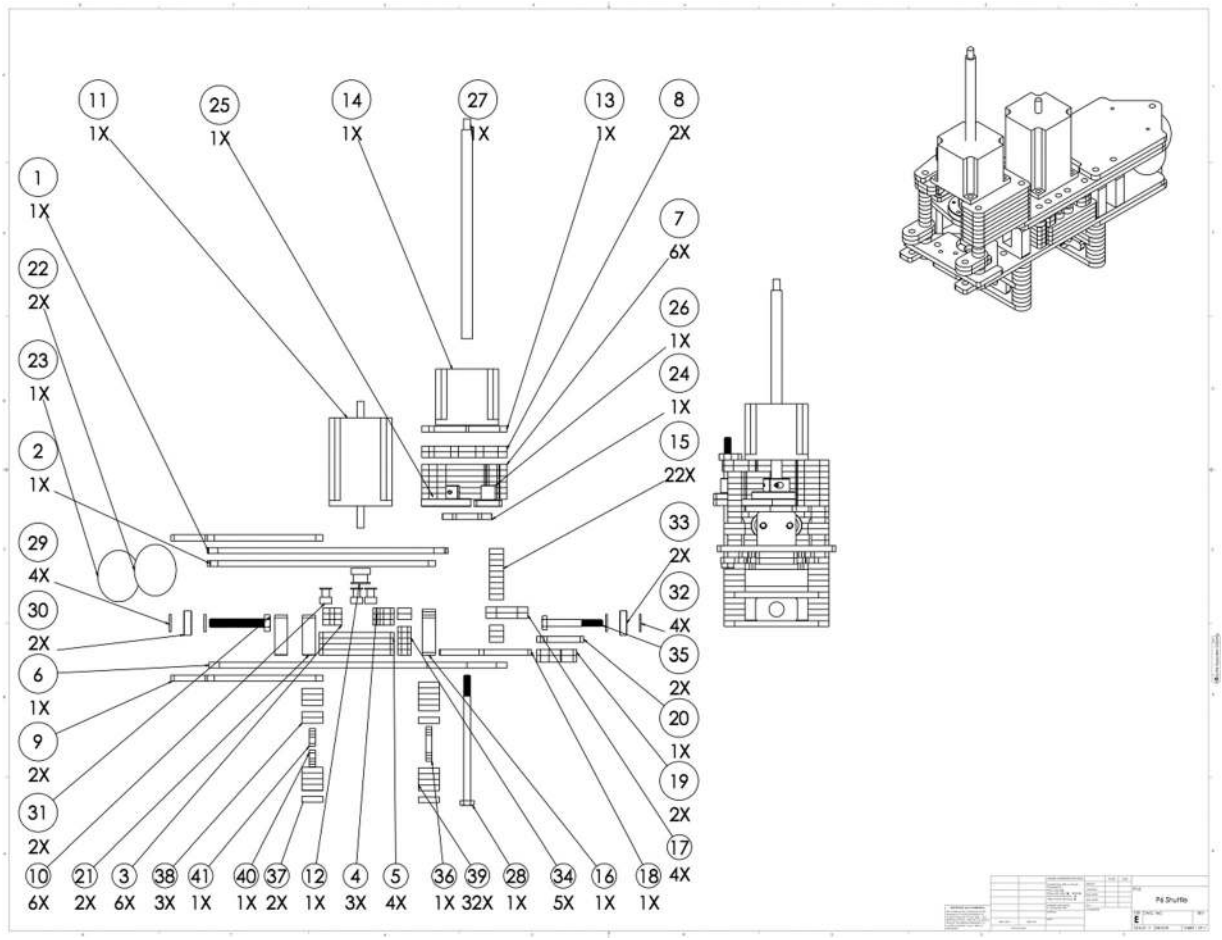

Fig. 3 P6 shuttle: The shuttle assembly, driven along the *Y*-axis via timing belt, includes a noncaptive stepper motor with a native step distance of 10 μm used as a microextrusion pump. A laser attachment, in current configuration, allows for light-induced activation of printing material pre-extrusion.

$$\text{Rotor inertia} \geq \frac{J_L}{J_O * i^2} \tag{4}$$

The rotor inertia for the designed bioprinter has a ratio of 0.012 well below the threshold value of 5. With a permissible inertia ratio established, the next parameter of interest is the required output torque. The load torque is defined by Eq. (5) and F is defined in Eq. (6), where W is the weight of the load. Alpha is the angle load and is measured in relation to the ground, in this case 90 deg. P_B relates to the same pitch value as used in the inertia calculation and T_B relates the breakaway torque, which is the amount of torque necessary to begin threading a screw when no other forces are present

$$T_L = \left(\left(\left(F * \frac{P_B}{2 * \pi}\right) * 1.1\right) + T_B\right)\left(\frac{1}{\eta * 0.01}\right) \tag{5}$$

$$F = F_A + W(\sin(\alpha) + \mu * \cos(\alpha)) \tag{6}$$

F_A defines a force actively working against the gantry's direction of travel and in this case goes to zero. Thus, substituting into known values of Eqs. (5) and (6) yields: $F = 11$ lbs and $T_L = 147.1$ oz $*$ in. Typical leadscrew efficiencies range from 30% to 70%. Values of 30%, 50%, and 70% were used to examine potential opportunities to eventually improve the platform performance. With the Z axis motor suitability established, the X and Y axes are also validated. While the X axis drives a heavier load, this is mitigated by the kinetic friction of steel bearing on a steel sheet. Based on the equation for F, the effective force driven by the X axis motor is ~1 lb, due to a kinetic friction coefficient of 0.05 mitigating the force needed to move the ~22 lb structure. The Y-axis load is likewise reduced from 9.5 lb to 0.95 lb due to similar kinetic friction coefficients between the steel bearing and aluminum rod.

Pump Output. The printer design utilizes a syringe clamped in place to extrude a cell-laden liquid. While the prototype design is limited to 5 mL of fluid, the clamp could be adapted to larger volume syringes. The printer emphasizes single use syringes to facilitate simple printing setup and clean-up. A noncaptive motor capable of generating 800 N was purchased to achieve extrusion. Using digital calipers to measure the inner diameter of the syringe to be 12.35 mm, the cross-sectional area was calculated to be 119.79 mm^2. Recognizing that pressure is merely a force applied to an area, 800 N imposed on an area of 119.79 mm^2 results in 6.7 MPa of pressure. While cell printing usually occurs at ~30 kPa, the operational range of this pump allows highly viscous fluids to be extruded as well [23].

Linear Calibration of *X*-, *Y*-, *Z*-, and *A*-Axis. Each stepper motor used in this platform possesses a native resolution of 200 steps per revolution. The total distance traveled per revolution is related to the diameter of driving pulleys attached to the drive shafts. While the initial settings are 200 steps per revolution, physical switches on the stepper motor drivers allow for microstepping ratios up to 1:125.

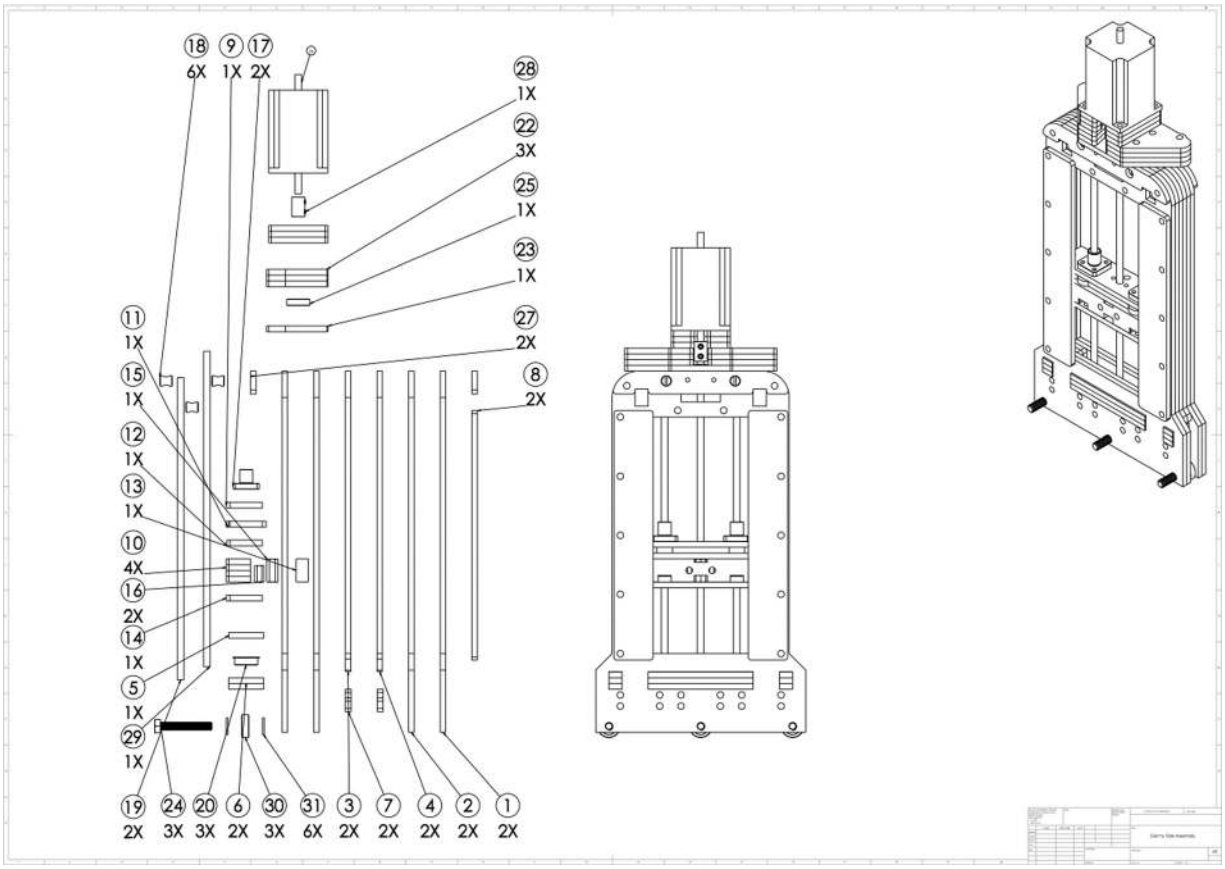

Fig. 4 V2 rocket assembly: For ease of viewing, the assembly depicts half of the gantry structure that actuates the shuttle along the 120 mm *Z*-axis working envelope via threaded rod coupled with a stepper motor. Two linear bearings and shaft-quality precision ground rods ensure vertical motion fidelity.

The stepper motors along the *X* and *Y* axes should be similar in their steps per millimeter due to the identical setup of their drive mechanisms. Both utilize 20-tooth MXL pulleys with a pitch diameter of 0.509 in to drive the gantry uniaxially. To determine the steps per unit measurement, the overall distance of one revolution is divided by the number of effective steps per revolution. With a microstepper ratio of 1:10, 2000 steps are required to complete one revolution. A 0.509 in diameter correlates to a 1.5991 in perimeter. Converted to millimeters, this gives 40.61714 mm per revolution. By dividing the steps per revolution, the steps per unit measurement are calculated to be 49.24 steps per millimeter or approximately 20 μm per step. While used as a starting calibration, this value was tuned to 47 steps per millimeter, giving an average percent error of 0.08% when moved across a 10 mm space. The *Y*-axis displays similar trends. Theoretically, with a maximum ratio of microstepping (1:125), the printer can achieve 1.6 μm positional resolution.

The second way to calibrate the printer is to use MACH3's built in calibration tool. The user dictates the distance MACH3 should tell the motor to travel. After the motor positions itself at the designated location, the user indicates what the actual distance traveled was. MACH3 then calculates and suggests a new step per unit value. This tool can be extremely helpful in establishing and validating motor setting; however, unless high-resolution tools are available, the uncertainty error associated with measurements will cause MACH3 to suggest new values with each iteration. These proof-of-concept calibrations use measuring calipers with readouts to the nearest hundredth of a millimeter. Due to this uncertainty, MACH3 suggestions fluctuated between 46.331 (steps/revolution) and 47.246 (steps/revolution). This step range results in a 0.017 mm distance uncertainty per revolution. The suggested values correlate with the independent calibration performed outside of MACH3.

The *Z*-axis and *A*-axis motors utilize threaded rods to generate motion, differing the calculations required to calibrate. The *Z*-axis utilizes an imperial lead screw with a $\frac{1}{4}$ in 20 thread, which results in a 0.05 in linear movement per revolution. Imperial screws nomenclature dictates that the first value is the screw diameter and the second value is the number of threads per inch. Therefore, on a $\frac{1}{4}$ in 20 screw, it takes 20 revolutions to travel 1 in or 0.05 in per revolution. Converting this to millimeters equates to 1.27 mm. As mentioned previously, the *Z*-axis requires greater control than the *X* or *Y*. Therefore, the *Z* axis utilizes a 1:125 microstepping ratio, resulting in 25,000 steps per revolution. The *Z* axis translates 1 mm of linear movement every 19685.04 steps imparting a theoretical step interval of 50.8 nm. This step count generated an average error percent of 0.04 over 10 mm of linear motion.

The *A* axis is actuated along a M10-2 threaded rod. The metric nomenclature indicates each thread is 2 mm apart, or a 2 mm linear movement occurs every revolution. Similar to the X and Y stepper motors, a 1:10 micro step ratio was imposed. This created a linear actuator with one micrometer step size with similar error percentages to the *Z* axis motion. With a 1 μm step distance and a syringe with an inner diameter of 12.35 mm, the *A* axis is able to extrude as little as 0.12 μL of fluid.

Volumetric Calibration. The volumetric calibration of the pump is a more convoluted process dependent on the properties of the bio-inks processed such as viscosity, swelling factors, and coalescence resistance. However, these various factors manifest via a

Fig. 5 Representative photographs of 3D-printed samples

single variable: the filament diameter. This diameter can be modified within the Skeinforge interface page of the 3D printing add-on for MACH3 and the slicing program prevents overlap from occurring. As such, the pathing for a 1 mm filament diameter will be less packed than the pathing for a 0.1 mm filament diameter. This likewise will influence the number of layers to be printed. It is assumed that a single pixel (single-step extrusion event ejecting the physically limited smallest volume possible) printed into a fluid substrate will form a spheroid structure. Thus, the filament diameter is also the layer height, imposing that the 0.1 mm diameter filament will need ten times the number of layers to complete an identical structure to the 1 mm filament. The optimization between resolution and speed is application dependent and will need to be assessed for each printing material and job.

Design Processing

Three-Dimensional Geometries. A few simple geometries were developed as proof-of-concept for tridimensional positional and extrusion control (Fig. 2) using an over-the-counter antibiotic ointment as the substrate. Initial prints through the needle were unsuccessful as the printing platform traversed the print path too quickly for the extruded material to leave the syringe and attach to the substrate. This indicates that the motor and pump output will need to be further optimized for each printing material (Figs. 3–5).

Osteogenic Differentiation of Adult Stem Cells. This printer was designed as a preliminary project for single-step deposition and activation of mesenchymal adult stem cells. Qureshi et al. [21] conducted a study that functionalized silver nanoparticles can be light activated via the on-board laser mediating micro-ribonucleic acid delivery resulting in increased alkaline phosphatase activity and mineralization of the mesenchymal stem cells. The study can potentially be reproduced with single-step seeding and light-mediated osteogenesis. Due to the reduced power of the laser pointer, an extended period of approximately 30–40 s of exposure is expected to occur before cellular printing.

Conclusion

A cost-effective 3D bioprinter utilizing microextrusion for academic research was designed, fabricated, and characterized. Acrylic was chosen as a structural material due to the ease of machining and its optical clarity. The developed platform delivers 3D spatial control with movement step intervals of approximately 21.3 μm in the X and Y axes and roughly 50.8 nm in the Z axis. Due to the relatively low power requirements of this novel bioprinting system, stepper motors were used to actuate tridimensional motion. By incorporating a noncaptive stepper motor into the gantry, a simple, yet effective syringe pump was implemented. The syringes used to dispense fluids are regarded as a single use attachment to the platform. Associated with the pump and cellular deposition is the laser light-activation attachment. The light-activation attachment is angled such that the cells are irradiated with light before being printed and it offers inline capability to active nanoparticle functionalized cells. While the employed design was chosen for ease of implementation, for future studies in which the optical line of sight between the laser and syringe is inhibited, the laser can be placed such that it irradiates vertically into the waiting substrate. Additional future work may incorporate a higher resolution laser device, allowing for side-by-side co-culturing of multiple light-activated tissues.

Acknowledgment

The 4-Axis Lightening Stepper Motor Driver Kit from Probotix provided four stepper motors, four stepper motor drives, a breakout board, and power supply. A noncaptive stepper motor and M10-2 threaded rod were obtained from Nanotech. Mach 3 is a computer numeric control interface software developed by Artsoft. Nuri Erginer created a 3D printing add-on for the Mach 3 software suite and provided it to the public free of charge. Half-inch thick Chemcast acrylic sheets were acquired from Delvies Plastics, while 0.22 in OPTIX acrylic sheets were purchased from Lowes or Home Depot, dictated by store inventory.

References

[1] Kim, W. R., Smith, J. M., Skeans, M. A., Schladt, D. P., Schnitzer, M. A., Edwards, E. B., Harper, A. M., Wainwright, J. L., Snyder, J. J., Israni, A. K., and Kasiske, B. L., 2012, "OPT/SRTR 2012 Annual Data Report: Liver," Am. J. Transplant., **14**(S1), pp. 69–96.

[2] Langer, R., and Vacanti, J., 1993, "Tissue Engineering," Science, **260**(5110), pp. 920–926.

[3] Mironov, V., Visconti, R. P., Kasyanov, V., Forgacs, G., Drake, C. J., and Markwald, R. R., 2009, "Organ Printing: Tissue Pheroids as Building Blocks," Biomaterials, **30**(12), pp. 2164–2174.

[4] Kaully, T., Kaufman-Francis, K., Lesman, A., and Levenberg, S., 2009, "Vascularization—The Conduit to Viable Engineered Tissues," Tissue Eng., Part B, **15**(2), pp. 159–169.

[5] Rauh, J., Milan, F., Gunther, K.-P., and Stiehler, M., 2011, "Bioreactor Systems for Bone Tissue Engineering," Tissue Eng., Part B, **17**(4), pp. 263–280.

[6] Prima Di, M., Coburn, J., Hwang, D., Kelly, J., Khairuzzaman, A., and Ricles, L., 2016, "Additively Manufactured Medical Products—The FDA Perspective," 3D Print. Med., **2**(1), pp. 1–6.

[7] Melchels, F., Domingos, M., Klein, T., Malda, J., Bartolo, P., and Hutmacher, D., 2012, "Additive Manufacturing of Tissues and Organs," Prog. Polym. Sci., **37**(8), pp. 1079–1104.

[8] Carvalho, J., Carvalho, P., Gomes, D., and Goes, A., 2013, "Innovative Strategies for Tissue Engineering," *Advances in Biomaterials Science and Biomedical Applications*, InTech, Rijeka, Croatia, pp. 295–313.

[9] Henmi, C., Nakmura, M., Nishiyama, Y., Yamaguchi, K., Mochizuki, S., Takiura, K., and Nakagawa, H., 2008, "New Approaches for Tissue Engineering: Three Dimensional Cell Patterning Using Inkjet Technology," Inflammation Regener., **28**(1), pp. 36–40.

[10] Wust, S., Godla, M., Muller, R., and Hofmann, S., 2014, "Tunable Hydrogel Composite With Two-Step Processing in Combination With Innovative Hardware Upgrade for Cell-Based Three-Dimensional Bioprinting," Acta Biomater., **10**(2), pp. 630–640.

[11] Boland, T., Xu, T., Damon, B., and Cui, X., 2006, "Application of Inkjet Printing to Tissue Engineering," Biotechnol. J., **1**(9), pp. 910–917.

[12] Billiet, T., Vandenhaute, M., Schelfhout, J., Vlierberghe, S., and Dubruel, P., 2012, "A Review of Trends and Limitations in Hydrogel-Rapid Prototyping for Tissue Engineering," Biomaterials, **33**(26), pp. 6020–6040.

[13] Boland, T., Mironov, V., Gutowska, A., Roth, E., and Markwald, R., 2003, "Cell and Organ Printing 2: Fusion of Cell Aggregates in Three-Dimensional Gels," Anat. Rec., Part A, **272**(2), pp. 497–502.

[14] Cui, X., and Boland, T., 2009, "Human Microvasculature Fabrication Using Thermal Inkjet Printing Technology," Biomaterials, **30**(31), pp. 6221–6227.

[15] Hong, S., Song, S. J., Lee, J., Jang, H., Choi, J., Park, Y., and Sun, K., 2013, "Cellular Behavior in Micropatterned Hydrogels by Bioprinting System Depended on the Cell Types and Cellular Interaction," J. Biosci. Bioeng., **116**(2), pp. 224–230.

[16] Wilson, C., and Boland, T., 2003, "Cell and Organ Printing 1: Protein and Cell Printers," Anat. Rec., Part A, **272A**(2), pp. 491–496.

[17] Nakamura, M., Kobayashi, A., Takagi, F., Watanable, A., Hiruma, Y., Ohuchi, K., Iwasaki, Y., Horie, M., Morita, I., and Takatani, S., 2005, "Biocompatible Inkjet Printing Technique for Designed Seeding of Individual Living Cells," Tissue Eng., **11**(11–12), pp. 1658–1666.

[18] Guillotin, B., Souquet, A., Catros, S., Duocastella, M., Pippenger, B., Bellance, S., Bareille, R., Rémy, M., Bordenave, L., Amédée, J., and Guillemot, F., 2010, "Laser Assisted Bioprinting of Engineered Tissue With High Cell Density and Microscale Organization," Biomaterials, **31**(28), pp. 7250–7256.

[19] Toma, C., Pittenger, M., Cahill, K., Byrne, B., and Kessler, P., 2002, "Human Mesenchymal Stem Cells Differentiate to a Cardiomyocyte Phenotype in the Adult Murine Heart," Circulation, **105**(1), pp. 93–98.

[20] Guillotin, B., and Guillemot, F., 2011, "Cell Patterning Technologies for Organotypic Tissue Fabrication," Trends Biotechnol., **29**(4), pp. 183–190.

[21] Qureshi, A., Monroe, W., Dasa, V., Gimble, J., and Hayes, D., 2013, "miR-148b-Nanoparticle Conjugates for Light Mediated Osteogenesis of Human Adipose Stromal/Stem Cells," Biomaterials, **34**(31), pp. 7799–7810.

[22] Murphy, S., and Atala, A., 2014, "3D Bioprinting of Tissues and Organs," Nat. Biotechnol., **32**(8), pp. 773–785.

[23] Nair, K., Gandhi, M., Khalil, S., Yan, K., and Marcolongo, M., 2009, "Characterization of Cell Viabilility During Bioprinting Processes," Biotechnol. J., **4**(8), pp. 1168–1177.

[24] Walker, P., Jimenez, F., Gerber, M., Aroom, K., Shah, S., Harting, M., Gill, B., Savitz, S., and Cox, C., 2010, "Effect of Needle Diameter and Flow Rate on Rat and Human Mesenchymal Stromal Cell Characterization and Viability," Tissue Eng., Part C, **16**(5), pp. 989–997.

[25] Chang, C., Boland, E., Williams, T., and Hoying, J., 2011, "Direct-Write Bioprinting Three-Dimensional Biohybrid Systems for Future Regenerative Therapies," J. Biomed. Mater. Res., Part B, **98**(1), pp. 160–170.

[26] Peltola, S., Melchels, F., Grijpma, D., and Kellomaki, M., 2008, "A Review of Rapid Prototyping Techniques for Tissue Engineering Purposes," Ann. Med., **40**(4), pp. 268–280.